Mid-infrared soliton and Raman frequency comb generation in silicon microrings

Tobias Hansson,[1,2] Daniele Modotto,[1] and Stefan Wabnitz[1,*]

[1]*Dipartimento di Ingegneria dell'Informazione, Università di Brescia, via Branze 38, 25123 Brescia, Italy*

[2]*Department of Applied Physics, Chalmers University of Technology, SE-41296 Göteborg, Sweden*

*Corresponding author: stefan.wabnitz@unibs.it

We numerically study the mechanisms of frequency comb generation in the mid-infrared spectral region from cw-pumped silicon microring resonators. Coherent soliton comb generation may be obtained even for a pump with zero linear cavity detuning, through suitable control of the effective lifetime of free carriers from multiphoton absorption, which introduces a nonlinear cavity detuning via free-carrier dispersion. Conditions for optimal octave spanning Raman comb generation are also described.   © 2014 Optical Society of America

OCIS codes: (230.5750) Resonators; (190.4410) Nonlinear optics, parametric processes; (190.4380) Nonlinear optics, four-wave mixing; (190.4970) Parametric oscillators and amplifiers.

http://dx.doi.org/10.1364/OL.39.006747

Optical frequency comb generation using nonlinear optical microresonators offers an intriguing alternative to mode-locked lasers. A host of potential applications, including biomedical and environmental spectroscopy, arise in the mid-infrared (MIR) range of the spectrum [1]. Planar microring resonators that can be fabricated directly on CMOS compatible chips are particularly interesting for their low cost and mass manufacturing potential. The natural candidate for implementing a chip-scale, MIR frequency comb source is silicon, because of its 10^2 higher nonlinearity compared to silica, coupled with vanishing two-photon absorption (TPA) and associated free-carrier absorption (FCA) and dispersion (FCD) for photon energies below the silicon half-bandgap [2]. Recent experiments have demonstrated that silicon-chip-based MIR frequency comb generation is critically dependent upon the possibility of reducing the lifetime of free carriers generated by three-photon absorption (3PA) [3].

In this work we present a numerical study of MIR frequency comb generation in silicon microresonators, which demonstrates that a proper control of the free-carrier lifetime (FCT) may enable a new route for stable soliton self-mode-locking of the comb. Indeed, multiphoton-absorption-induced FCD introduces a dynamic nonlinear cavity detuning, which replaces the need for a nonzero linear cavity detuning [4,5]. We also predict the highly efficient generation of MIR Raman frequency combs [6] from silicon microresonators.

Time dynamics of frequency comb generation in silicon microresonators is described by a generalized nonlinear envelope equation for the field envelope $A[\sqrt{W}/m]$, which includes linear loss and dispersion, the Kerr effect, Raman scattering, TPA and 3PA, FCA and FCD [2,5–10],

$$
\left[\frac{1}{v_g}\partial_\tau - D + \alpha + i\delta_0 + \frac{\sigma}{2}(1+i\mu)\langle N_c(\tau)\rangle\right]A(\tau,t)
$$
$$
= f_0 + ik_0\left(1 + i\tau_{sh}\frac{\partial}{\partial t}\right)p_{NL}^{(3)}(\tau,t), \quad (1)
$$

coupled with the evolution equation for the averaged carrier density $\langle N_c(\tau)\rangle$,

$$
\partial_\tau\langle N_c(\tau)\rangle = \frac{\beta_{TPA}(\omega)}{2\hbar\omega_0}\langle|A|^4\rangle + \frac{\gamma_{3PA}}{3\hbar\omega_0}\langle|A|^6\rangle - \frac{\langle N_c(\tau)\rangle}{\tau_{eff}}, \quad (2)
$$

where τ is a continuous (slow) temporal variable that replaces the round-trip number, $v_g = c/n_g$ and n_g are the group velocity and refractive index at the pump carrier frequency ω_0, $k_0 = \omega_0/c$, $\tau_{sh} = 1/\omega_0$, and t is a retarded (fast) time. In Eq. (2), brackets denote average over the cavity circulation time t_R: $\langle X(\tau)\rangle = (1/t_R)\int_{-t_R/2}^{t_R/2}X(t,\tau)dt$, so that Eq. (2) describes the buildup of carriers within the cavity over many round trips, supposing that the FCT $\tau_{eff} \gg t_R$. The group-velocity dispersion (GVD) operator D reads as

$$
D = \sum_{m\geq 2}\frac{i^{m+1}}{m!}\left(\frac{\partial^m\beta}{\partial\omega^m}\right)\frac{\partial^m}{\partial t^m}. \quad (3)
$$

In Eq. (1) the linear loss coefficient $\alpha = \alpha'/L$ with $\alpha' = \alpha_d L + \theta/2$, α_d represents distributed cavity loss and θ is the transmission coefficient between the resonator of length L and the bus waveguide. Moreover, σ is the FCA coefficient, μ is the FCD coefficient, β_{TPA} is the TPA coefficient, $\delta_0 = \bar{\delta}_0/L = (\omega_R - \omega_0)t_R/L$ is the linear cavity detuning (where ω_R is the closest linear cavity resonance to the pump frequency ω_0), $f_0 = (\sqrt{\theta}/L)A_{in}$ and A_{in} the injected cw pump amplitude. The cavity boundary conditions impose the field to be t-periodic with period t_R, i.e., $A(\tau,t) = A(\tau, t+t_R)$. The nonlinear polarization reads as

$$
p_{NL}^{(3)} = n_2[(1-\gamma_R)\big(\eta \otimes (|A|^2 A) + ir_3|A|^4 A
$$
$$
+ A^3\exp(-2i\omega_0 t)/3\big) + \gamma_R\int_{-\infty}^{t}h_R(t-t')|A(t')|^2 dt'], \quad (4)
$$

where $\otimes$ denotes convolution product, n_2 is the nonlinear index, and γ_R is the Raman fraction coefficient associated with the response function,

$$h_R(t) = H(t) \frac{\tau_1^2 + \tau_2^2}{\tau_1 \tau_2^2} \exp(-t/\tau_2) \sin(t/\tau_1), \qquad (5)$$

where $H(t)$ is the Heaviside function, $\tau_1 = 10.2$ fs and $\tau_2 = 3.03$ ps. Whenever pumping the transverse electric (TE) mode, the scalar Raman gain coefficient $\gamma_R = g_R \Gamma_R/(n_2 k_0 \Omega_R) = 0.018$, where we used $n_2 = 9 \times 10^{-18}$ m^2/W and the peak parallel Raman gain value $g_R = 2 \times 10^{-10}$ m/W at the wavelength $\lambda_0 = 1.55$ μm, the gain bandwidth $\Gamma_R/\pi = 105$ GHz, and the peak gain frequency shift $\Omega_R/2\pi = 15.6$ THz. On the other hand, when the input cw pump is coupled to the transverse magnetic (TM) mode, the parallel Raman gain vanishes in silicon [11], hence $\gamma_R = 0$. In Eq. (4) $\eta = \delta(t) + r_2(t)$, where $r_2(t) = \mathcal{F}^{-1}(\hat{r}_2(\omega))$ is related to the frequency-dependent TPA coefficient as $\hat{r}_2(\omega) = \beta_{\text{TPA}}(\omega)c/(2\omega_0 n_2)$, where the wavelength dependence of the TPA coefficient $\beta_{\text{TPA}}(\omega)$ was estimated using the analytical approximation of [12]. TPA vanishes for wavelengths larger than 2.2 μm. Moreover, we supposed a wavelength-independent 3PA contribution, which is represented in Eq. (4) by the coefficient $r_3 = \gamma_{\text{3PA}}c/3\omega_0 n_2$.

We tailored the linear dispersion and effective area properties of the silicon microrings for efficient MIR frequency comb generation. This involves a suitable design of the microresonator radius and cross section. In fact, the shape of the frequency combs can be controlled through the geometric contribution to the effective refractive index of the cavity mode. Figure 1(a) illustrates examples of dispersion profiles for the TE and TM modes of a 50 μm radius ring, with a 1 μm wide, 500 nm thick waveguide, computed from a commercial mode solver (for details, see [13]). Whereas in Fig. 1(b) we show the dispersion profiles for a 1.5 μm wide, 1.5 μm thick waveguide: as can be seen, the absolute value of dispersion is considerably reduced with respect to the previous case of a smaller waveguide, in particular as far as the TE mode is concerned. Moreover, for the larger waveguide the GVD of both modes remains anomalous for $\lambda > 2$ μm. The effective area of the TM mode of the large (small) waveguide is equal to 1.37 μm^2 (0.32 μm^2) at $\lambda_0 = 2.6$ μm; whereas for the TE modes $A_{\text{eff}} = 1.23$ μm^2 ($A_{\text{eff}} = 0.32$ μm^2).

Based on our design of the spatial mode properties of the microrings, we numerically simulated the temporal dynamics of MIR frequency comb generation by solving Eqs. (1)–(5) in the frequency domain as a set of coupled
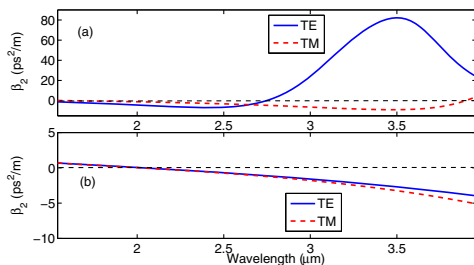
ordinary differential equations for the resonator modes, with computationally efficient evaluation of the four-wave mixing terms in the time domain via the fast Fourier transform routine [14]. This approach permits to easily include in the modeling the frequency dependence of nonlinear terms, such as TPA, as well as of the effective mode area. We used a quantum noise input (one photon per mode), and considered a microresonator with quality factor $Q = \pi n_g/\alpha'\lambda_0 = 3.5 \times 10^5$ operating in the critical-coupling regime, i.e., we set $\alpha' = \theta = 2\alpha_d L$, so that $\theta = 0.004$ at $\lambda_0 = 2.6$ μm. We pumped with $P_{\text{in}} = 1$ W of input cw power and used $\sigma = 3.7 \times 10^{-21}$ m^2, $\mu = 4.7$, and $\gamma_{\text{3PA}} = 0.025$ cm^3/GW^2 [15–17].

Let us consider first the dynamics of frequency comb generation when pumping the TM mode. Figure 2(a) shows the temporal evolution of the intracavity intensity in the TM mode of the large waveguide of Fig. 1(b) for a pump wavelength $\lambda_0 = 2.6$ μm and no cavity detuning, i.e., $\delta_0 = 0$: the corresponding $t_R = 3.83$ ps and the free spectral range (FSR) is equal to 261 GHz. As can be seen, a stable soliton pattern is generated, which is composed of a bound soliton quadruplet and an additional isolated soliton. The corresponding temporal (spectral) profile of the power coupled out of the resonator is shown in Figs. 3(a) and 3(b).

The spectral intensity in Fig. 2(b) shows that a transient primary frequency comb after about 1 ns is followed by the generation of a stable and coherent soliton comb. The evolution of the field energy in Fig. 2(c) shows the relaxation toward a stable fixed value associated with the $N = 5$ soliton ensemble. In order to arrive to a stable multisoliton comb, it is necessary to properly adjust the
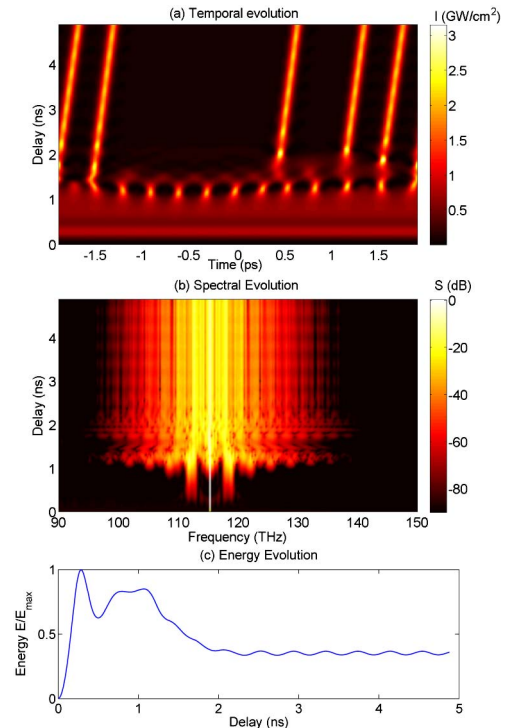

Fig. 2.   Soliton frequency comb generation from TM mode of large microring as in Fig. 1(b): (a) temporal evolution; (b) spectral evolution of intracavity intensity; (c) energy evolution. Here $\tau_{\text{eff}} = 320$ ps and $\lambda_0 = 2.6$ μm.

Fig. 1.   GVD β_2 for the TE (solid blue) and TM (dashed red) modes of a silicon ring resonator with (a) inner radius $a = 49.5$ μm, outer radius $b = 50.5$ μm, and $h = 0.5$ μm (see [13]) or (b) for waveguide dimensions of 1.5 μm × 1.5 μm.
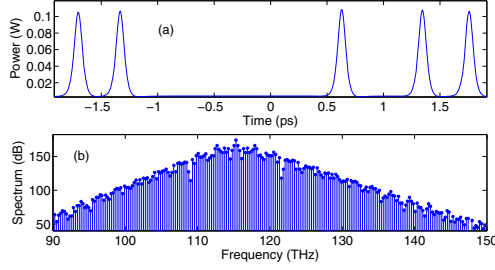
Fig. 3.   Output soliton frequency comb as in Fig. 2: (a) power and (b) spectral profile.

FCT (here $\tau_{\text{eff}} = 320$ ps). As shown in [3,18], this can be achieved by tuning the reverse bias voltage applied to a PIN structure embedding the microring: $\tau_{\text{eff}} = 320$ ps corresponds to about 2 V bias.

Here the mechanism for soliton generation is, first, the noise-induced modulation instability of the cw cavity solution, which leads to a periodic pulse pattern. This is followed by the development of nonlinear cavity detuning introduced by FCD, which leads to the generation of isolated cavity solitons. Figure 4(a) shows the τ evolution toward a stable fixed point of the comb energy and detuning $\delta_{\text{FCD}} = \sigma\mu\langle N_c\rangle L_d/2 \approx 0.95$, where $L_d \equiv t_0^2/|\beta_2(\lambda_0)|$ and $t_0 = 65$ fs. The resulting soliton amplitude may be approximated as $|A(t)| = \eta\,\text{sech}(\rho t/t_0)$ [19], where $\eta = \sqrt{\sigma\mu\langle N_c\rangle/\gamma}$, $\rho = \sqrt{2\delta_{\text{FCD}}}$, and $\gamma = 2\pi n_2/\lambda_0$. One predicts for Figs. 2 and 3 the soliton peak intensity $I_s = \eta^2 \simeq 2$ GW/cm^2 and temporal duration $t_s = 1.763\sqrt{|\beta_2(\lambda_0)|/(\sigma\mu\langle N_c\rangle)} \simeq 83$ fs, in excellent agreement with the numerics. Thus, FCD leads to cavity soliton generation via the development of a suitable nonlinear cavity detuning.

The number of cavity solitons N may be further controlled by introducing a (fixed) nonzero linear cavity

detuning: Fig. 5 shows that a stable $N = 2$ soliton comb is obtained with $\bar{\delta}_0 = 0.05$, so that $\delta_0 L_d = 0.72$. Correspondingly, the FCD-induced detuning is reduced to $\delta_{\text{FCD}} = 0.58$.

For the formation of a stable soliton comb, the FCT should be comprised between a lower and an upper bound. For example, as τ_{eff} grows larger than a certain critical value, a Hopf bifurcation into an oscillating comb is observed, see Fig. 6 where $\tau_{\text{eff}} = 400$ ps. In this case the comb exhibits τ-periodic breathing: spectral broadenings in Fig. 6(b) are associated with the emergence of a quasi-periodic pulse train. Moreover, Figs. 6(c) and 4(b) show that the intracavity energy exhibits periodic explosions.

Self-induced soliton comb generation is also observed for different microring geometries and pump wavelengths. Figure 7, obtained when pumping the TM mode of the small microring of Fig. 1(a) at $\lambda_0 = 2.2$ μm, shows that the long-term behavior of a $N = 6$ soliton comb is subject to strongly dissipative dynamics: soliton annihilation (upon collision) is accompanied by the nearly simultaneous soliton creation at a different temporal position, so that the total soliton number is conserved, to keep the FCD-induced detuning unchanged. Figures 7(b) and 7(c) show that, in correspondence with each soliton annihilation/creation event, a transient spectral broadening occurs, accompanied by a small energy peak.

When pumping the TE mode of the microring, the parallel Raman gain dramatically changes the nature of the generated frequency comb. To ensure that the peak of Raman gain at 15.6 THz shift from the pump occurs for an integer multiple (e.g., $M = 61$) of the cavity FSR, we slightly increased the ring diameter (from 50 to 51.3 μm). Figure 8(b) shows that a Raman frequency comb is
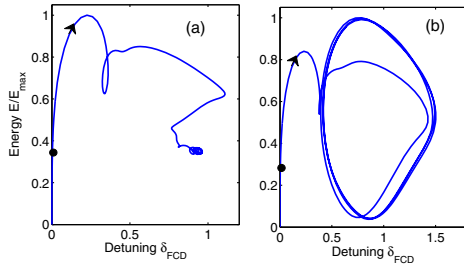

Fig. 4.   Comb energy versus FCA-induced detuning: (a) as in Fig. 2; (b) as in Fig. 6. The black dot indicates the initial values and the arrow shows the direction of evolution.
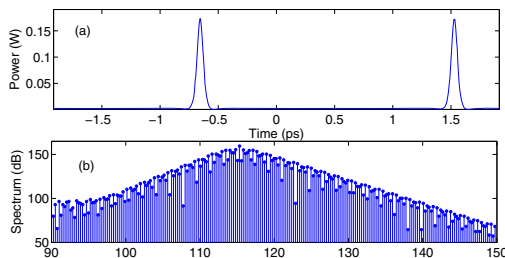

Fig. 5. $N = 2$ soliton frequency comb as in Fig. 3 with $\bar{\delta}_0 = 0.05$ and $\tau_{\text{eff}} = 190$ ps.
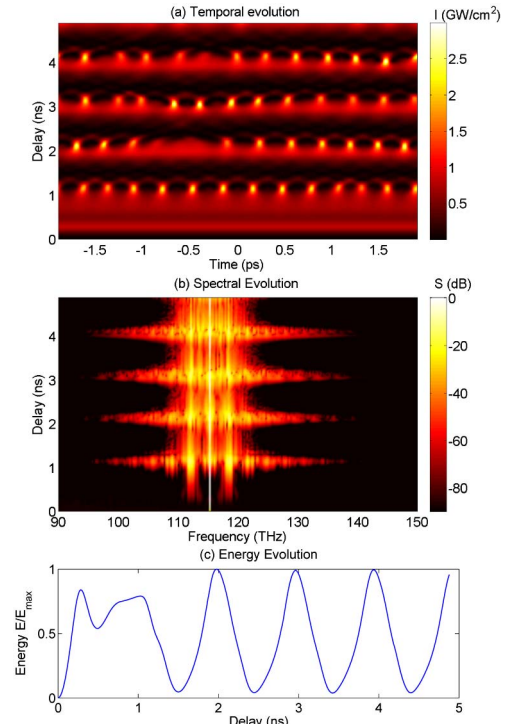

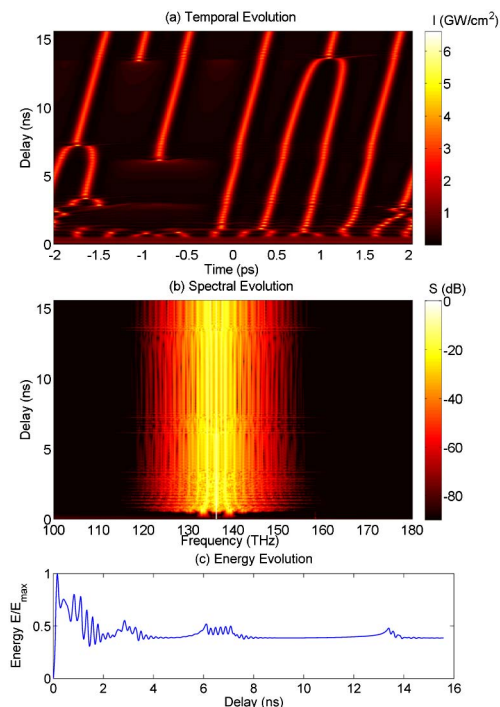Fig. 6.   Same as in Fig. 2, with $\tau_{\text{eff}} = 400$ ps.

Fig. 7.   Soliton frequency comb generation from TM mode of small microring as in Fig. 1(a): (a) temporal evolution; (b) spectral evolution of intracavity intensity; (c) energy evolution. Here $\tau_{\text{eff}} = 100$ ps and $\lambda_0 = 2.2$ μm.
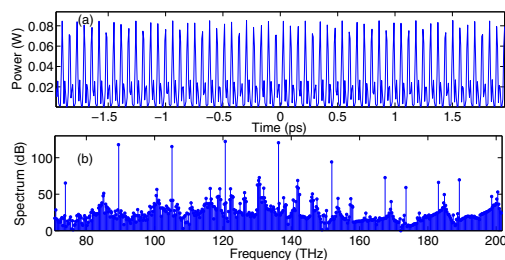

Fig. 8.   Raman frequency comb from TE mode of large microrings as in Fig. 1. Here $\tau_{\text{eff}} = 100$ ps and $\lambda_0 = 2.2$ μm; (a) power and (b) spectral profile.

generated, including three cascaded Raman Stokes lines of nearly equal intensity as the pump wave, as well as three anti-Stokes comb lines and a weaker fourth Stokes line at about 70 THz, for an octave-spanning Raman comb bandwidth in excess of 100 THz. Figure 8(a) shows that the Raman comb results in the generation of a train of pulses with about 15 fs duration, which by spectral post-processing could be compressed down to the single-cycle regime. Because of the large Raman gain (10^4 times the silica value) in silicon, Raman scattering remains the main comb generation mechanism also if the Raman gain shift is not precisely equal to a multiple of the FSR. Raman comb generation is also less sensitive to the

presence of free carriers than soliton comb generation, since no precise adjustment of the FCT is required.

In conclusion, a suitable control of the FCT may provide a mechanism for Kerr soliton frequency comb generation in the MIR with silicon microresonators. Octave-spanning Raman frequency comb generation was also predicted.

References

1. C. Y. Wang, T. Herr, P. Del'Haye, A. Schliesser, J. Hofer, R. Holzwarth, T. W. Hansch, N. Picque, and T. J. Kippenberg, Nat. Commun. **4**, 1345 (2013).
2. R. K. Lau, Y. Okawachi, M. R. E. Lamont, and A. L. Gaeta, "Effects of multiphoton absorption on parametric comb generation in silicon microresonators," in *Conference on Lasers and Electro-Optics*, San Jose, California, June 8–13, 2014, paper STh1I.4
3. A. G. Griffith, R. K. W. Lau, J. Cardenas, Y. Okawachi, A. Mohanty, R. Fain, Y. H. Daniel Lee, M. Yu, C. T. Phare, C. B. Poitras, A. L. Gaeta, and M. Lipson, "Silicon-chip mid-infrared frequency comb generation" arXiv:1408.1039 (2014).
4. T. Herr, V. Brasch, J. D. Jost, C. Y. Wang, N. M. Kondratiev, M. L. Gorodetsky, and T. J. Kippenberg, Nat. Photonics **8**, 145 (2014).
5. M. R. E. Lamont, Y. Okawachi, and A. L. Gaeta, Opt. Lett. **38**, 3478 (2013).
6. F. Couny, F. Benabid, P. J. Roberts, P. S. Light, and M. G. Raymer, Science **318**, 1118 (2007).
7. M. Haelterman, S. Trillo, and S. Wabnitz, Opt. Commun. **91**, 401 (1992).
8. V. V. Kozlov and S. Wabnitz, J. Opt. Soc. Am. B **27**, 1707 (2010).
9. T. Hansson, D. Modotto, and S. Wabnitz, Phys. Rev. A **88**, 023819 (2013).
10. L. Yin and G. P. Agrawal, Opt. Lett. **32**, 2031 (2007).
11. Q. Lin, O. J. Painter, and G. P. Agrawal, Opt. Express **15**, 16604 (2007).
12. A. D. Bristow, N. Rotenberg, and H. M. van Driel, Appl. Phys. Lett. **90**, 191104 (2007).
13. T. Hansson, D. Modotto, and S. Wabnitz, J. Opt. Soc. Am. B **31**, 1109 (2014).
14. T. Hansson, D. Modotto, and S. Wabnitz, Opt. Commun. **312**, 134 (2014).
15. R. K. W. Lau, M. R. E. Lamont, A. G. Griffith, Y. Okawachi, M. Lipson, and A. L. Gaeta, Opt. Lett. **39**, 4518 (2014).
16. S. Peart, N. Rotenberg, and H. M. van Driel, Appl. Phys. Lett. **93**, 131102 (2008).
17. T. Wang, N. Venkatram, J. Gosciniak, Y. Cui, G. Qian, W. Li, and D. T. H. Tan, Opt. Express **21**, 32192 (2013).
18. A. C. Turner-Foster, M. A. Foster, J. S. Levy, C. B. Poitras, R. Salem, A. L. Gaeta, and M. Lipson, Opt. Express **18**, 3582 (2010).
19. S. Wabnitz, Opt. Lett. **18**, 601 (1993).